INVESTIGATION OF SLIDING WEAR MECHANISM AND CAUSES ON A DIESEL APPLICATION ROLLER FOLLOWER

Rafael Amboss Pinto[1], Avelino Elias Martins de Souza[1],
Vitor Atsushi Shimada[1], Sérgio Medeiros dos Santos[2]

[1]Robert Bosch Ltda.
[2]Universidade Federal do Paraná

E-mails: rafael.pinto@br.bosch.com, avelino.souza@br.bosch.com,
vitor.shimada@br.bosch.com, medeirosergio@hotmail.com

ABSTRACT

The cam-roller system, commonly used in heavy duty truck applications, consists in a roller follower actuated by the engine camshaft to transmit the cam linear movement. At the application under study, the contact to the cam is through a roller made of 100Cr6 bearing steel. In a Dynamometer test, two out of six rollers presented an unacceptable level of wear, characterized by formation of pitting and spalling, typical of contact fatigue wear. Plastic deformation caused by high friction sliding was also detected by SEM analysis. A macrography of roller's top surface, polished and etched with Nital, shown discrete regions where sliding occurred, with non-tempered martensite spots surrounded by severely tempered martensite regions, evidencing intermittent sliding and rolling movements. The wear mechanism correlates with information from literature about "plasticity-dominated sliding wear" caused by high friction sliding between surfaces, leading to material removal by contact fatigue through two different coexistent mechanisms. Other possible causes of failure were discarded, hence it can be stated that the wear cause is inadequate lubrication of engine oil, such as low lubricity and particles in suspension, associated with unequal thermal expansion, studied by FEA, leading to roller/cam sliding and resulting in plastic deformation, microstructure changes on roller surface and particles detachment by low cycle contact fatigue failure at the end of the test.

INTRODUCTION

Cam-roller system operation overview

A typical driving system in Diesel engines consists in a roller follower (Figure 1) actuated by the engine camshaft, transmitting the cam linear movement to other sub-systems [1]. During the cam up-stroke, an axial force of ~19kN is transmitted to the cam-roller contact. During the cam down-stroke and base circle periods, ~500N is transmitted. Hence, the axial force applied to the roller follower – which is transmitted to the roller/cam contact – varies from ~19kN to ~500N each cycle, which lasts ~30ms (Figure 2).
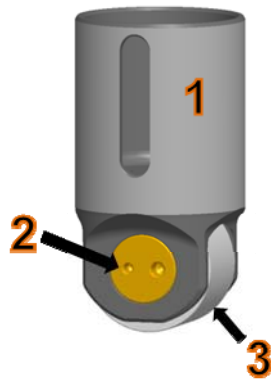
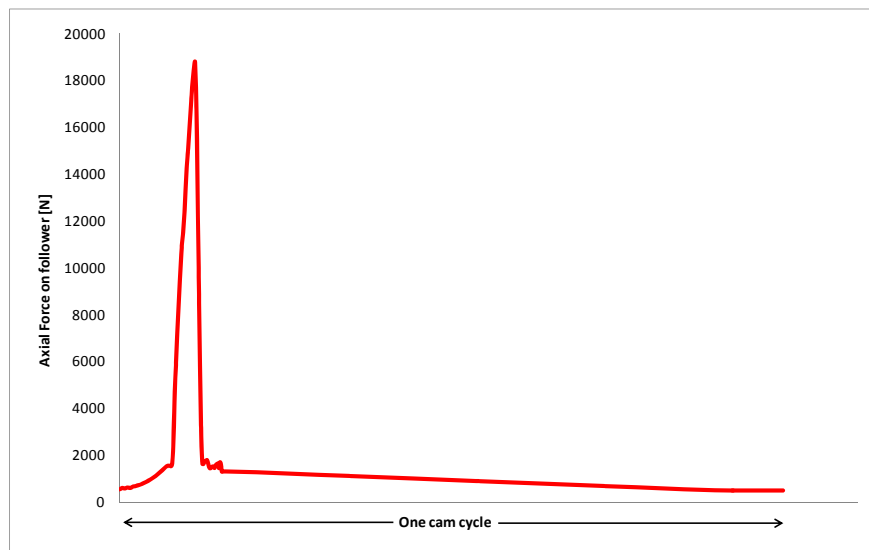**Figure 1 – Roller follower.**

Figure 2 – Axial force variation on roller follower during one cam cycle.

The main load to which the roller is submitted is contact stress on the interface with the cam. The contact is non-conformal, which increases the magnitude of the hertzian stress. The roller is made of steel 100Cr6, similar grade as SAE 52100, typically used for ball bearings [2]. It is used in the quenched and tempered condition.

The roller follower (Figure 1), consists in 3 parts: follower body (Figure 1 – "1"), axle pin (Figure 1 – "2"), which is pressed into the follower body, and roller (Figure 1 – "3"), which rotates freely around the axle pin. The contact between the roller and the axle pin operate as a sliding bearing, lubricated by the conventional engine lube oil, from the same reservoir that lubricates the combustion chamber piston. For this driving group, the lube oil is pumped, so it can reach the recommended flow to lubricate and cool the tribological contacts.

Problem description

As a validation program for an internal project, tests were carried out to ensure reliability on the follower manufactured on the new production site. One of the tests, carried out on dynamometer by the customer, resulted in excessive wear on 2 from a set of 6 rollers. "Severe wear" is characterized by material removal from the roller track, through formation and progress of contact fatigue pitting or spalling. The maximum admissible wear ("medium wear") is characterized by initial pitting formation, without evolution over operation time, and

running traces marked on roller track center. The "severely worn" rollers, shown on Figure 3, were from cylinders 1 and 6. The other four rollers from this set presented "light wear", described as "Slight running traces on the roller track surface". Figure 4 shows a SEM analysis of the worn rollers, evidencing contact fatigue and plastic deformation, which indicates that sliding between surfaces occurred.
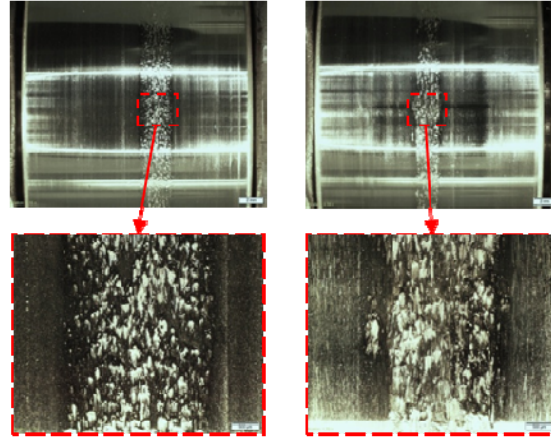

Figure 3 – Stereoscope images from worn rollers: cyl. 1 at left pictures and cyl. 6 at right pictures.

Evidences of sliding wear:

a) smoothed surface.

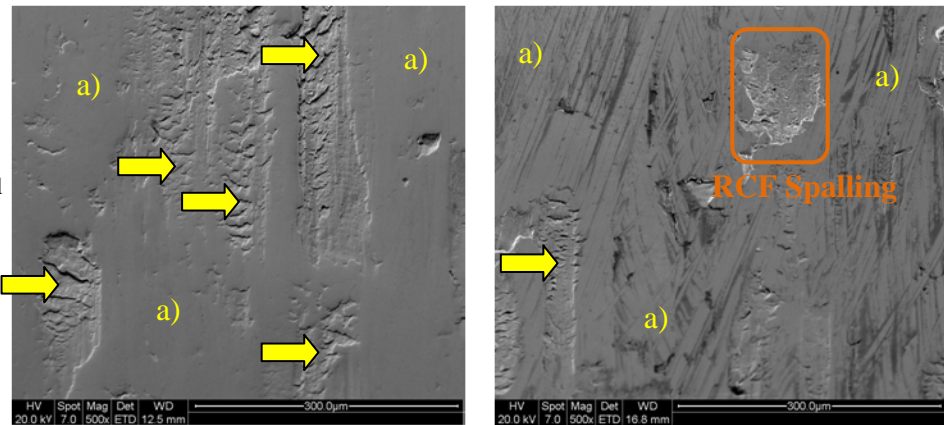b) shingles due to local seizure with lost material due to adhesion (➡)

Figure 4 - SEM images from 2 rollers (cyl. 1, left picture) and (cyl. 6, right picture), pointing the evidences of the wear mechanisms identified.

Then, the objective of this work is to determine the wear mechanism and understand the causes for such a severe wear found of the rollers.

1. THEORETICAL BASIS

RCF (rolling contact fatigue) occurs with contact stress e.g. Hertzian stress applied (in this case, non-conform contact between cam and roller). It causes a e.g. Mises stress distribution from surface to the core (in where shear stress is included), see Figure 5. The maximum Mises stress spot occurs not in the surface, but some microns deep. With higher slip, the maximum stress point comes closer to the surface due to higher shear stress applied. Micro-slip is a typical phenomenon on rolling contacts, since there is deformation on both surfaces. It is further discussed on [3].
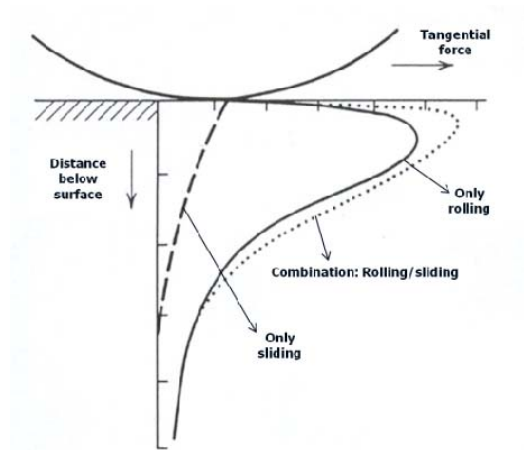
Figure 5 – Hertzian stress distribution from surface to core when non-conformal contact is applied.

Sliding wear, in this case precisely "plasticity-dominated sliding wear", may be caused after protection layers consisting of lubricant additives and/or oxidation are worn. On nanoscale, the local material strength of the asperity contacts is exceeded and nano-particles break out. These nano-particles increase the abrasive wear due to micro furrowing seen as smoothed surface. With high affinity between materials without any lubrication or oxide layer, and high temperature, the asperity contacts can also built a chemical bonding [4] (welding) and lead also to nano-particles and nano welding and consequently to shingles on microscale.

Irregular surface caused by surface defects (contact fatigue or indentation by hard particles) is plastically deformed during sliding, frequently inside the RCF pitting. Adhesive microscale wear can be verified by material transfer from one part on the other and is evidenced in the SEM as shingles. Other mechanism of plasticity is known as delamination, which consists in crack nucleation below surface and its propagation parallel to the surface [4].

The two mechanisms of wear converge when the plastic deformation of material surface is discussed. Due to sliding with high friction coefficient, plastic deformation takes place on the worn surface [3]. The strain is higher as closer to the material surface, according to Figure 6. The mechanism can be understood as a low cycle fatigue phenomenon.
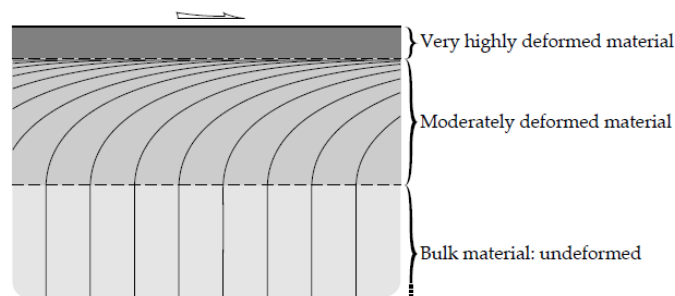

Figure 6 – Plastic deformation shape due to sliding wear.
Source: [3]

Plasticity-dominated sliding wear and contact fatigue wear mechanisms are so close that it may be discussed either on "Sliding wear" chapter, as on reference [4], or on "Fatigue wear" chapter, as on reference [3].

A point of convergence between sliding wear and contact fatigue wear is notable: when shear stress is applied to the surface (i.e. sliding), it contributes to increase the magnitude of the Mises stress and bring it closer to the surface, where heterogeneities (e.g. roughness) are likely. As shown on Figure 7, the crack then starts on surface and propagates from surface to bulk material, along slip planes or dislocation cell boundaries [3]. In this case, the phenomenon can be understood as low or high cycle fatigue depending on presence or absence of plastic deformation.
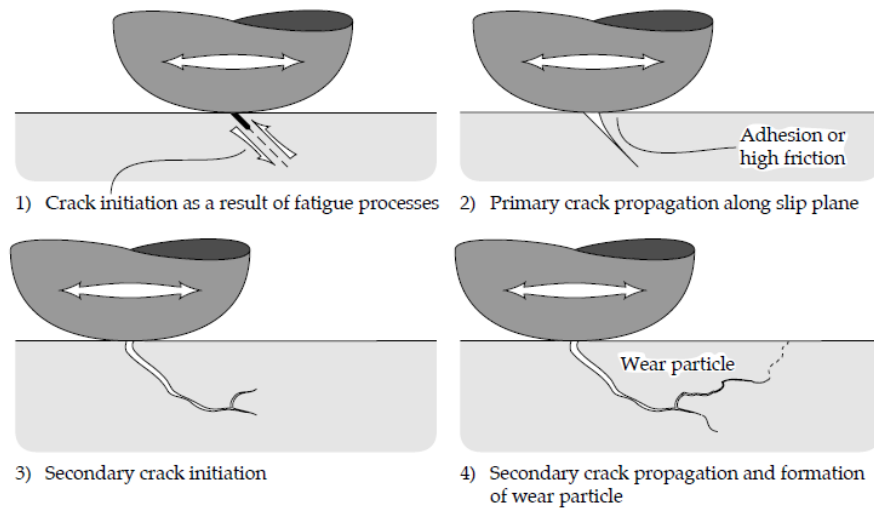

1) Crack initiation as a result of fatigue processes
2) Primary crack propagation along slip plane
3) Secondary crack initiation
4) Secondary crack propagation and formation of wear particle

Figure 7 – Crack propagation from surface to bulk material along a slip plane. Source: [3]

According to [5], spalling-starter cracks don't come from pittings coalescence. They come actually from material defects (e.g. inclusions) and the main propagation mode is II (see Figure 8), since mode I is impossible due to absence of traction forces normal to the surface: only a constant compressive force acts on the crack faces. Mode III has a secondary role on the crack propagation. When spalling originates from subsurface, the main cause is frequently high Hertzian stress solely, and not poor lubrication [5].
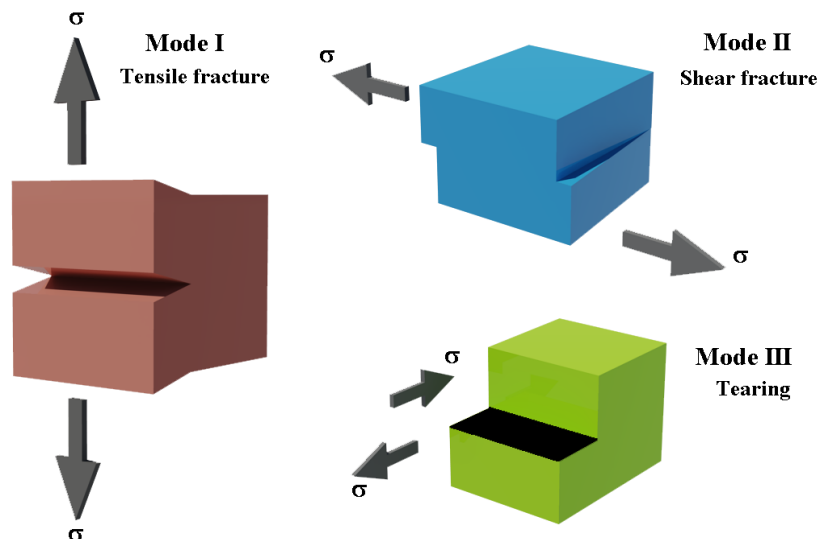

Figure 8 – 3 possible modes of crack propagation. Spalling cracks propagate mainly by mode II, with some movements of mode III. Source: [6].

Pitting is considered the least severe mode of RCF, and consists in microcracks formation related to the friction orientation. A proof of that is the opposite orientation of these microcracks on the adendum and on the dedendum driver gear (see Figure 9) [5].
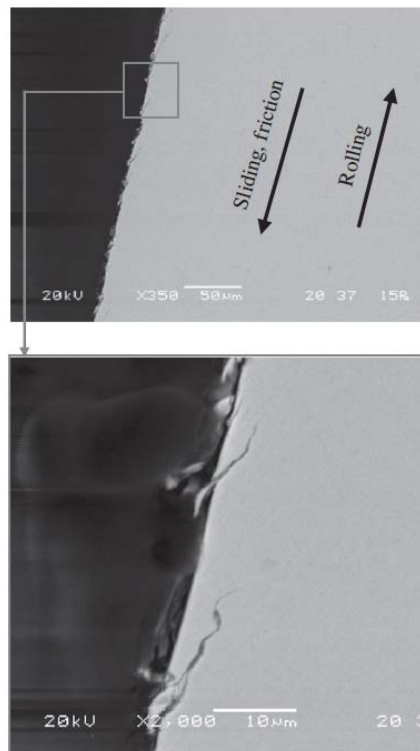

Figure 9 – Microcracks in a dedendum driver gear tooth. The microcracks orientation are opposite to the friction. Source: [5]

In summary, the three forms of contact fatigue beginning that are interesting for this work are:
1. Through severe plastic deformation due to high shear stress on the surface with poor lubrication. The crack is formed on the "moderately deformed material" region from Figure 6 and propagates parallel through mode II to the surface until changing its direction and reaching the surface, releasing a material particle.
2. Through pittings that start on surface, due to high stress (Figure 5) applied on regions with heterogeneities, such as roughness valleys. The crack then propagates in an angle around 30° with the surface (Figure 7). This mode occurs generally when lubrication is not adequate and asperities contact occur [5].
3. Inclusion or material defect starts a crack due to high contact stress below surface (Figure 5) and it propagates through mode II. This can occur without asperities contact, when lubrication regime is adequate: elasto-hydrodynamic (EHL) [5].

Burn and re-hardening is another contributor to sub superficial cracks formation and propagation. This phenomenon initiate with the presence of high temperature that may cause austenitizing of material on surface. Since the thermal conduction of steel is high, in association to high grade of alloy elements present on bearing steels such as 100Cr6, the cooling is fast enough to form martensite, that remains in a non-tempered condition and is more resistant to Nital etching, appearing in white color on the metallography. Around the non-tempered martensite spots, the temperature is not high enough to austenitize the steel, but high enough to temper it further than the manufacturing process did, decreasing hardness. These regions are less resistant to Nital etching, appearing in dark color on the metallography.

Figure 10 shows a typical transverse microstructure of the roller, made of martensitic 100Cr6, on which "burn and rehardening" occurred. This local phase transformation, which involves volume change [7], in association with hardness difference between non-tempered martensite, directly in contact with severely-tempered martensite, causes local tensile stress which, summed to stress caused by contact and sliding, decreases the fatigue lifetime, forms spalling and releases particles.

Steel AISI 52100, similar to 100Cr6, was tested under lubrication of several mineral and synthetic oils. It was noticed that for oils of the same family, the contact fatigue lifetime is increased as higher is the viscosity. Naturally, high viscosity increases the losses by hydrodynamic friction. So, the design must reach a compromise between these two factors. It is mentioned also the secondary martensite, here called "non-tempered martensite", shown on "re-hardening" region of Figure 10, as one leading factor to cracks nucleation [8].

Figure 10 – Typical microstructure of "burn and re-hardening". Etch: Nital.

2. EVALUATION METHODS

For determining the main cause for roller excessive wear, four possible causes were proposed, discussed and investigated. The investigation methods for them are described at this section.

The material used at the investigation is the roller after a dynamometer test cycle. The chemical composition is given on Table 1 [9]. For the microstructure evaluation, samples were prepared using conventional metallographic technique, etched with Nital and observed at the optical microscope OLYMPUS BX51M.

Table 1 - 100Cr6 chemical composition (%). Source: [9]

C	Si	Mn	P	S	Ni	Cr	Cu
0.95 - 1.10	0.15 - 0.35	0.25 - 0.40	0.03	0.025	0.3	1.35 - 1.65	0.3

For the wear mechanism investigation, the top surface and the transverse section of the roller were observed on the Scanning Electron Microscope (SEM) FEI QUANTA 200, also equipped with the Energy Dispersive X-Ray Spectrometer (EDS) OXFORD X-ACT, used to evaluate the composition of particle attached to the axle pin. The top rolling track was observed without any surface preparation at SEM. Also for the top rolling track, conventional metallographic technique was applied, the sample was etched with Nital and observed on the Stereoscope OLYMPUS SZX16.

To calculate the clearances after thermal deformation considering the real geometry, a Finite Element Analysis (FEA) was carried out, using the software ABAQUS CAE™ version 6.12-3.

To assess the statistical distribution of the clearance between the follower and its guide, a tolerance analysis with MonteCarlo simulation, as described on the introduction of [10], was carried out using software MiniTab™.

3. RESULTS AND DISCUSSION

The first hypothesis is that Hertzian stress may be increased by increase of the Normal Force due to higher friction coefficient on follower/guide interface (marked in red on Figure 11), e.g. due to follower roundness deviation, caused by thermal expansion of axle pin. Since the P-Bronze material of the axle pin has a higher thermal expansion coefficient than the steel, with increase of follower temperature, the axle pin has its length increased (Figure 12). As it is attached to follower legs, they tend to open, causing deformation, which affects the follower's roundness on regions identified as "Higher stiffness" and "Lower stiffness 2" on Figure 12.
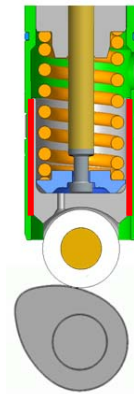

Figure 11 - Contact follower/guide in red.

A static FEM simulation was performed to evaluate the follower assembly behavior under heating. On the region "Higher stiffness" from Figure 12, the roundness deviation is smaller than 1µm. On region "Lower stiffness 2" the follower roundness deviation is around the magnitude of 10µm when heated to typical temperature peaks found on engine oil (see b-a on Figure 13). Moreover, peak temperatures are not enough to cause severe thermal deformations, since time is needed for the parts to reach thermal balance. Simulation assumed the peak temperature as constant, being more severe than reality.
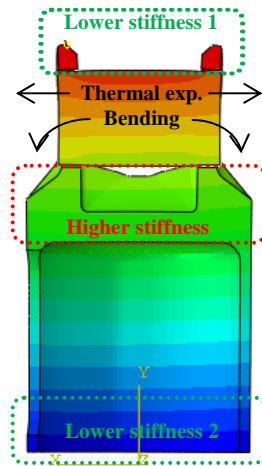
Figure 12 – FEM thermal expansion simulation showing bending of axle pin.

Considering that the guide increases its diameter regularly (perfectly round), the clearance tends to decrease on "Lower stiffness 2" region. The clearances between follower and its guide are usually at the magnitude of 60µm on both "Lower" and "Higher" stiffness regions. The tolerance combination of extreme values for diameters allows clearances as low as the magnitude of 20 µm. The process has high capability, thus it is known that extreme tolerance values in combination have very low probability to happen. Hence, to evaluate the real possibility of the follower to get seized on the guide, a stack-up analysis was made to compare the simulated clearance after typical peak temperature of engine oil (taking into account the roundness deviation and thermal expansion of follower and its guide) to the ambient temperature condition. The real capability of the follower diameter was considered, while a conservative value was assumed for the guide capability. In this way it is possible to quantify the real clearance being manufactured, while the "extreme tolerance approach" would be too conservative.
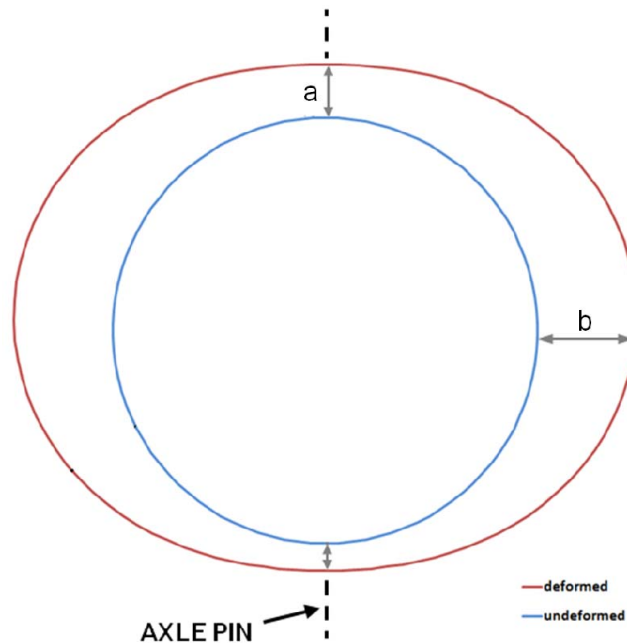

Figure 13 – Follower body thermal deformation on region identified as "Lower stiffness 2" from Figure 12.

The result of the stack-up analysis is shown on Figure 14. The normal distributions for clearance at ambient temperature and for clearance at simulated typical peak temperature of engine oil were plotted together. It can be stated that the roundness deviation at the typical peak temperature of engine oil tends to reduce the clearance only by some micrometers (Δ), comparing to the ambient temperature condition. The influence on guide/follower friction coefficient is insignificant for such a slight reduction. The probability of having the clearance equal to zero is not significant. Moreover, the guides and followers only presented light wear.
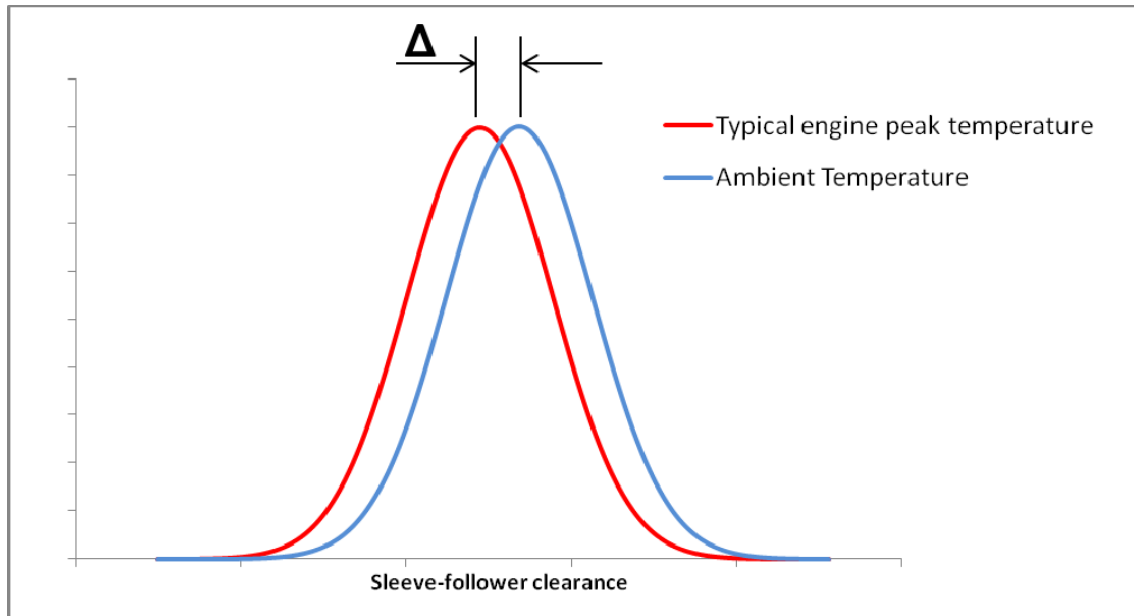

Figure 14 – Normal distribution for clearance at ambient temperature and after typical engine oil temperature.

The second hypothesis is due to unequal thermal expansion coefficient between axle pin and roller, which leads the clearance to decrease as the follower temperature increases. Moreover, the higher stiffness region shown on Figure 12 tends to cause bending on the axle pin. These factors could lead to roller sticking, allowing slip between roller and cam. The seizure temperature was determined also by a FEM simulation: when 365°C is reached, the clearance between roller and axle is zero, considering the assembly on minimum tolerance case. This temperature is unlikely to be reached during engine operation. However, FEM static simulation doesn't take into account the effect of temperature on the oil lubricity, which can lead to seizure on a lower temperature due to inadequate lubrication, instead of clearance equals to zero.

Unfavorable lubrication condition (e.g. low lubricity or particles on oil) tends to stick the roller on axle pin, leading to cam/roller slip (instead of normal rolling). This leads to the discussion of a third hypothesis. The result of sliding on cam/roller interface is "Plasticity-dominated sliding wear" [4], evidenced on the surface of the roller shown on Figure 15 and Figure 16. Great similarity with the schematic drawing shown on Figure 6 can be noted on both figures, where the high friction caused plastic deformation, more severe as closer to the surface.
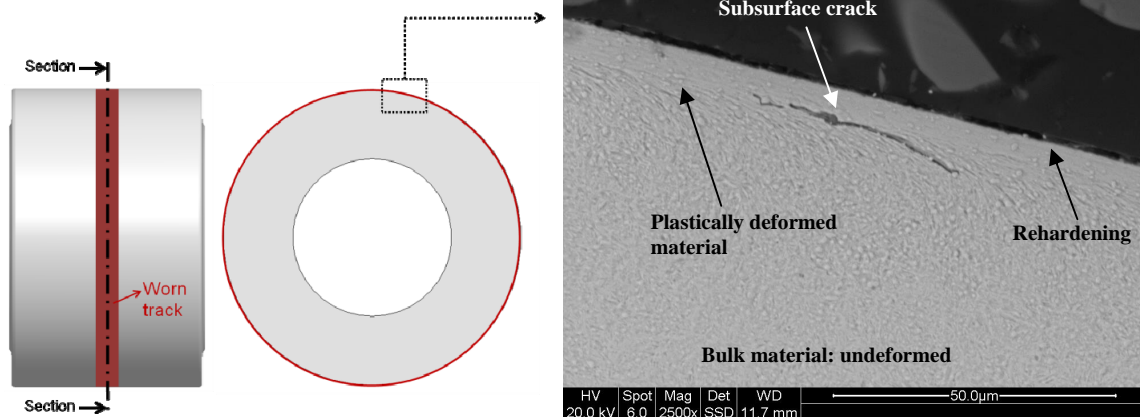
Figure 15 – SEM picture from transverse section parallel to rolling movement of roller, showing the plastically deformed material described on Figure 6 and the subsurface crack formation.
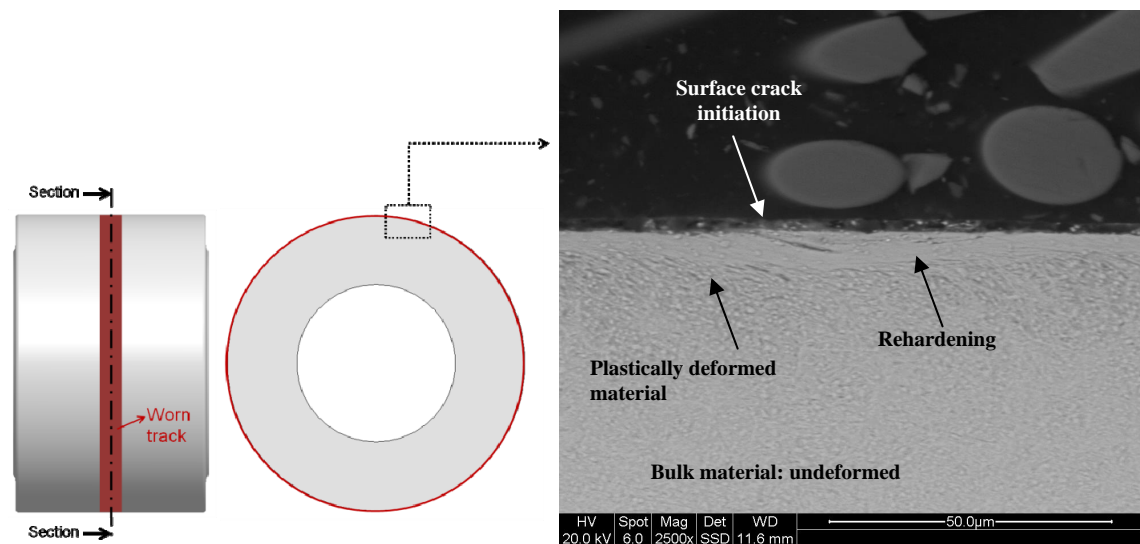

Figure 16 – SEM picture from transverse section parallel to rolling movement of roller, showing the plastically deformed material described on Figure 6 and the surface pitting formation.

Cracks formation at the subsurface, through contact fatigue form 1 (discussed on "Theoretical basis" section) is present on Figure 15. Wear by contact fatigue with pitting originating on the surface [5], form 2 of contact fatigue, is evidenced on Figure 16. Both figures show a section of the roller, parallel to its rolling direction. If the test has continued, the crack on Figure 15 would propagate through mode II and reach the surface, releasing a particle and forming a spall. Inadequate lubrication can be one leading factor to these forms of contact fatigue.

At the Material Laboratory the roller worn surface was manually polished, etched with Nital and observed on a multifocal stereoscope. An evidence of roller/cam slipping is depicted on Figure 17. Roller/cam slipping increases the local temperature severely. The roller was stuck on axle pin and slipping occurred intermittently, evidenced by the discrete worn sites. These worn sites appear in lighter color due to presence of non-tempered martensite (hard). Around the non-tempered martensite sites, the dark color evidences regions where the temperature was high enough to temper severely (causing soft spots), but not to austenitize and reharden. This interface of a hard microstructure (non-tempered martensite) with a soft microstructure

(severely tempered martensite) is likely to form cracks and start contact fatigue spalling. The crack may start on surface or below it, but in both cases it leads to spalling formation and material removal.

Due to lack of information about the cam worn regions, it is not possible to state if the slipping occurred on base circle or up-stroke region. Since on the up-stroke region of the cam the friction between cam and roller is higher due to higher normal force, rolling is more likely. On base circle, however, the friction is smaller and may be not enough to overcome the breaking torque of the roller, increased due to unfavorable lubrication condition.

Analyzing the axle pins, the grey region extends for almost its semi perimeter, starting from the lower region, where more intense contact with roller occurs (Figure 18). This is another evidence of roller sticking.

Figure 17 – Optical stereoscope picture from the top of worn roller track, polished and etched with Nital, showing rehardened regions (non-tempered martensite, hard) and burn regions (severely tempered martensite, soft).
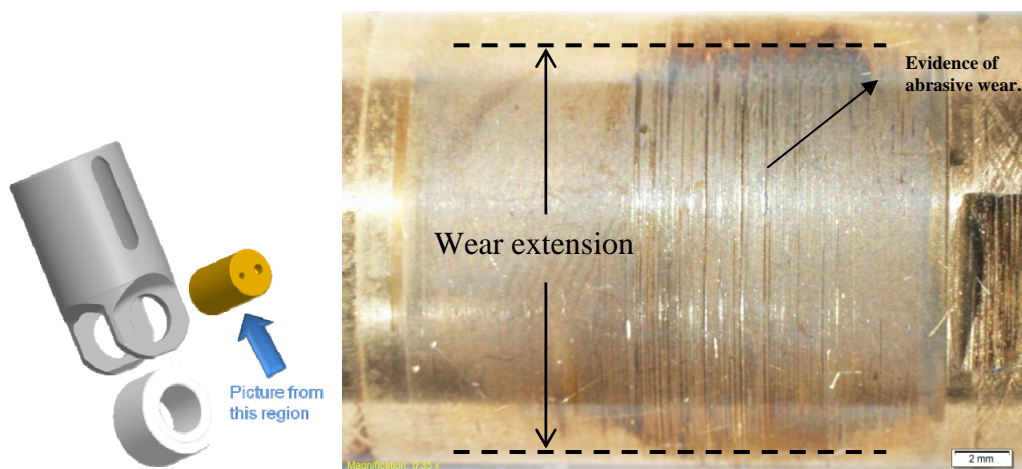

Figure 18 – Picture from multifocal stereoscope, showing the worn region of axle pin extending nearly to the semi perimeter. Abrasive wear due to particles was also observed.

An EDS composition analysis was performed, to identify the elements present on the particles attached to the axle pins. Four axle pins were analyzed, from the two worn rollers and from two rollers that passed the tests. All of them presented aluminum particles, one example can be seen on Figure 19. Figure 20 shows the SEM analysis of an axle pin from the same test and the particle identified as aluminum.
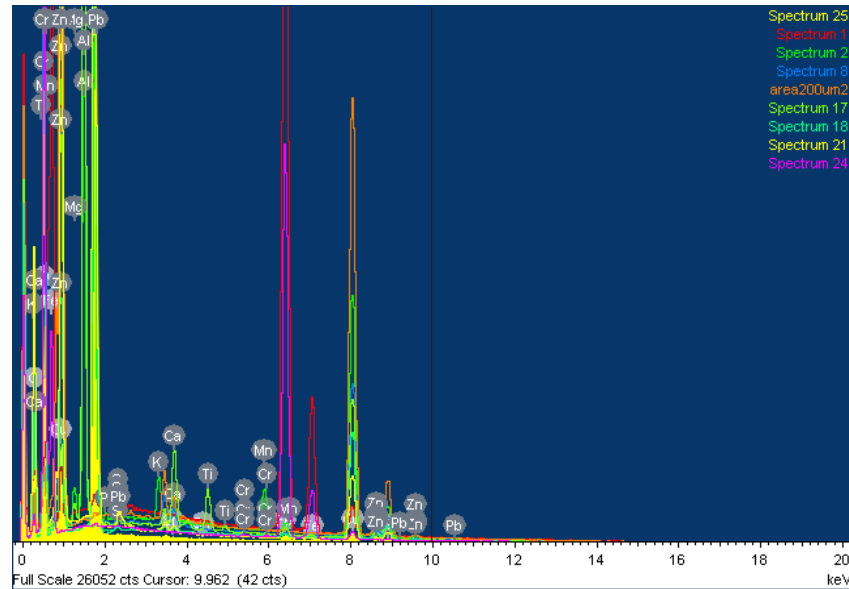

Figure 19 – EDS analysis of axle pin from a worn roller, exactly on one of the particles shown on SEM analysis at Figure 20.
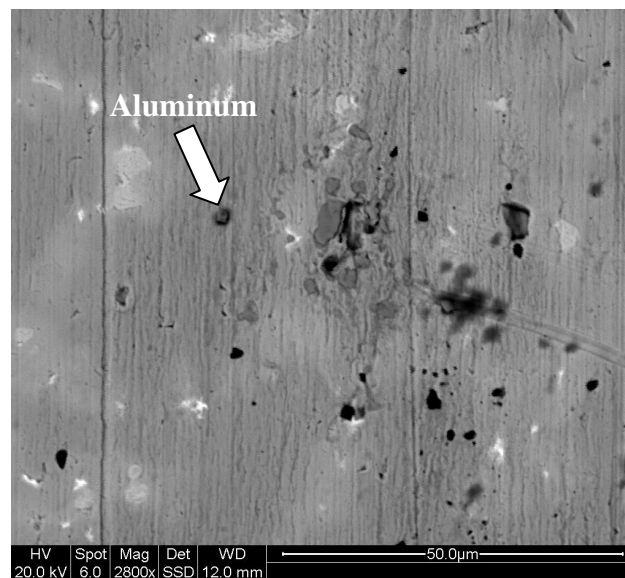

Figure 20 – SEM analysis of axle pin, pointing the Al particle.

In summary, statements about the three hypotheses are given below:
1. Wear on roller is due to increase of Hertzian stress on cam/roller interface, caused by abnormally high coefficient of friction between follower and its guide. FEM simulation and MonteCarlo statistical analysis proved that the deformation is not enough to cause interference between follower and its guide. This possible cause can be eliminated.
2. Unequal thermal expansion of axle pin decreases the clearance with roller and increases the coefficient of friction on this interface, causing roller sticking on axle pin and slipping

on cam. FEM simulation shown that the thermal expansion is not enough to cause interference on roller/axle interface. This possible cause can be eliminated.

3. Unfavorable lubrication condition (e.g. low lubricity or particles on oil) tend to stick the roller on axle pin, leading to cam/roller slip (instead of normal rolling). This cause was proved by wear mechanism analysis and by the EDS analysis on axle pin interface with roller, which found Aluminum particles from other engine parts. This indicates an unusually severe operation condition of the engine.

CONCLUSION

The scientific method of listing hypotheses and investigating them has lead to the statement about the wear mechanism and its causes. The investigation was supported by metallographic analyses with microscope and multifocal stereoscope, and SEM analysis with EDS. A FEA simulation of the roller follower thermal expansion was performed to evaluate the clearance decrease on roller/axle interface and on guide/follower interface. The follower roundness deformation under high temperature was discarded through a stack-up analysis.

The hypothesis 3 is the proved wear cause: on axle/roller contact, the high friction (due to particles on oil and/or low lubricity) associated with higher thermal expansion of axle pin (due to different material) increases the roller breaking torque and causes roller sticking. Aluminum particles were found on axle pins in interface with roller, what contributes significantly for roller sticking, in such a small clearance. Since the studied component has no part made of Aluminum, it certainly comes from other engine parts.

The wear mechanism analysis correlates with information from literature about "plasticity-dominated sliding wear" [4]. The coexistent forms of contact fatigue present on worn rollers are 1 and 2 as listed on the "Theoretical Basis" section, and both forms are associated with high friction coefficient due to asperities contact caused by unfavorable lubrication. No evidences were found of form 3 of contact fatigue. A clear correlation can be made by comparison between the deformed surface on Figure 15 and the schematic drawing on Figure 6.

During the last hours of test, lubrication problems occurred due to particles on oil and high temperature, enough to cause severe wear level. Moreover, the RCF lifetime tends to decrease with lower lubricant viscosity, highly influenced by the temperature [8]. Roller slipping also increases the temperature in such a way that is possible to form "re-hardened" regions, and the consequent microstructure changes may cause contact fatigue cracks initiation. The wear doesn't start exactly at the same moment for all rollers, reason why severe wear was found only on two out of six rollers. It is expected the evolution of wear on the other four rollers if the test had continued with the same lubrication conditions. Since plastic deformation is involved, the failure could only have occurred at the end of the test running time, otherwise the roller would have broken completely, given that the phenomenon is a low cycle fatigue failure.

REFERENCES

[1] ROBERT BOSCH GmbH; **Diesel-Engine Management**. 4th Edition, Plochingen: Bentley Publishers, 2005.

[2] BHADESHIA, H. K. D. H.; Steels for bearings. **Progress in Materials Science**. United Kingdom, v.57, p.268-345, 2012.

[3] STACHOWIAK, G. W.; **Engineering Tribology**. 3rd edition, Butterworth-Heinemann, 2005.

[4] HUTCHINGS, I. M.; **Tribology, Friction and Wear of Engineering Materials**. Burlington: Butterworth-Heinemann, 1992.

[5] SANTUS, C.; BEGHINI, M.; BARTILOTTA, I.; FACCHINI, M.; Surface and subsurface rolling contact fatigue characteristic depths and proposal of stress indexes. **International Journal of Fatigue.** Italy, v.45, p.71-81, 2012.

[6] ROCHA-RANGEL, E.; **Fracture Toughness Determinations by Means of Indentation Fracture.** Available at: http://www.intechopen.com/books/nanocomposites-with-unique-properties-and-applications-in-medicine-and-industry/fracture-toughness-determinations-by-means-of-indentation-fracture. Access on: May 1st 2014.

[7] COLPAERT, H.; Revisão Técnica: Silva A. L. V. C. **Metalografia dos produtos siderúrgicos comuns**. 4ª edição, São Paulo: Edgard Blucher, 2008.

[8] RICO, J. E. F.; BATTEZ, A. H.; CUERVO, D. G. Rolling contact fatigue in lubricated contacts. **Tribology International**, Spain, v.36, p.35-40, 2003.

[9] AMERICAN SOCIETY OF MATERIALS INTERNATIONAL (ASM). Properties and selection: Irons, Steels and High Performance Alloys. **In Metals Handbook**. 10th edition, Vol.1, p.454-455, 1990.

[10] GAO, J.; CHASE, K. W.; MAGLEBY, S. P.; A New Monte Carlo Simulation Method for Tolerance Analysis of Kinematically Constrained Assemblies. Available at: http://adcats.et.byu.edu/Publication/doc4/paper4.PDF. Access on: May 4th 2014.